

# Learning to Segment Moving Objects

Pavel Tokmakov · Cordelia Schmid · Karteek Alahari

Received: date / Accepted: date

**Abstract** We study the problem of segmenting moving objects in unconstrained videos. Given a video, the task is to segment all the objects that exhibit independent motion in at least one frame. We formulate this as a learning problem and design our framework with three cues: (i) independent object motion between a pair of frames, which complements object recognition, (ii) object appearance, which helps to correct errors in motion estimation, and (iii) temporal consistency, which imposes additional constraints on the segmentation. The framework is a two-stream neural network with an explicit memory module. The two streams encode appearance and motion cues in a video sequence respectively, while the memory module captures the evolution of objects over time, exploiting the temporal consistency. The motion stream is a convolutional neural network trained on synthetic videos to segment independently moving objects in the optical flow field. The module to build a “visual memory” in video, i.e., a joint representation of all the video frames, is realized with a convolutional recurrent unit learned from a small number of training video sequences.

For every pixel in a frame of a test video, our approach assigns an object or background label based on the learned spatio-temporal features as well as the “visual memory” specific to the video. We evaluate our method extensively on three benchmarks, DAVIS, Freiburg-Berkeley motion segmentation dataset and SegTrack. In addition, we provide an extensive ablation study to investigate both the choice of the training data and the influence of each component in the proposed framework.

**Keywords** Motion segmentation · Video object segmentation · Visual memory

## 1 Introduction

Video object segmentation is the task of extracting spatio-temporal regions that correspond to object(s) moving in at least one frame in the video sequence. The top-performing methods for this problem [15, 47] continue to rely on hand-crafted features and do not leverage a learned video representation, despite the impressive results achieved by convolutional neural networks (CNNs) for other vision tasks, e.g., image segmentation [51], object detection [52]. Very recently, there have been attempts to build CNNs for video object segmentation [8, 30, 33]. Yet, they suffer from various drawbacks. For example, [8, 33] rely on a manually-segmented subset of frames (typically the first frame of the video sequence) to guide the segmentation pipeline. The approach of [30] does not require manual annotations, but remains frame-based, failing to exploit temporal consistency in videos. Furthermore, none of these methods has a mechanism to *memorize* relevant features of objects in a scene. In this paper, we propose a novel framework to address these issues.

We present a two-stream network with an explicit memory module for video object segmentation (see Figure 1). The memory module is a convolutional gated recurrent unit (GRU) that encodes the spatio-temporal evolution of object(s) in the input video sequence. This spatio-temporal representation used in the memory module is extracted from two streams—the appearance stream which describes static features of objects in the video, and the temporal stream which captures the independent object motion.

The temporal stream separates independent object and camera motion with our motion pattern network (MP-Net),

---

The authors are at Inria.

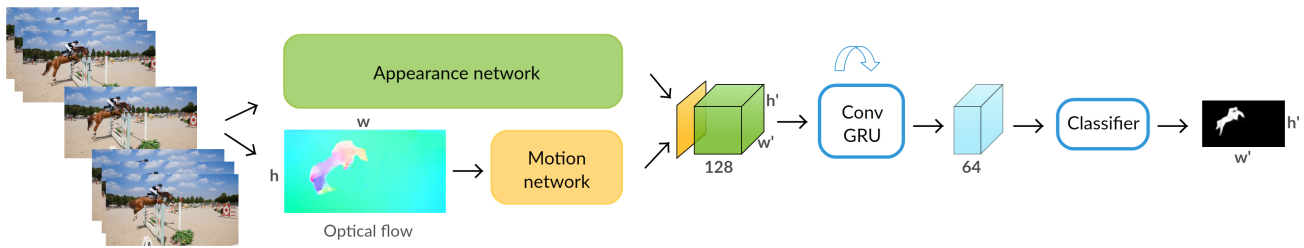


**Fig. 1** Overview of our segmentation approach. Each video frame is processed by the appearance (green) and the motion (yellow) networks to produce an intermediate two-stream representation. The ConvGRU module combines this with the learned visual memory to compute the final segmentation result. The width ( $w'$ ) and height ( $h'$ ) of the feature map and the output are  $w/8$  and  $h/8$  respectively.

a trainable model, which takes optical flow as input and outputs a per-pixel score for moving objects. Inspired by fully convolutional networks (FCNs) [13,40,54], we propose a related encoder-decoder style architecture to accomplish this two-label classification task. The network is trained from scratch with synthetic data [41]. Pixel-level ground-truth labels for training are generated automatically (see Figure 2(d)), and denote whether each pixel has moved in the scene. The input to the network is flow fields, such as the one shown in Figure 2(c). More details of the network, and the training procedure are provided in Section 4.2. With this training, our model learns to distinguish motion patterns of objects and background.

The appearance stream is the DeepLab network [9, 10], pretrained on the PASCAL VOC segmentation dataset, and it operates on individual video frames. With the spatial and temporal CNN features, we train the convolutional GRU component of the framework to learn a *visual memory* representation of object(s) in the scene. Given a frame  $t$  from the video sequence as input, the network extracts its spatio-temporal features and: (i) computes the segmentation using the memory representation aggregated from all frames previously seen in the video, (ii) updates the memory unit with features from  $t$ . The segmentation is improved further by processing the video in the forward and the backward directions in the memory unit, with our *bidirectional convolutional GRU*.

The contributions of the paper are three-fold. First we demonstrate that independent motion between a pair of frames can be learned, and emphasize the utility of synthetic data for this task (see §4). Second, we present an approach for moving object segmentation in unconstrained videos that does not require any manually-annotated frames in the input video (see §3). Our network architecture incorporates a memory unit to capture the evolution of object(s) in the scene (see §5). To our knowledge, this is the first recurrent network based approach for the video segmentation task. It helps address challenging scenarios where the motion patterns of the object change over time; for example, when an object in motion stops to move, abruptly, and then moves again, with potentially a different motion pattern. Finally,

we present state-of-the-art results on the DAVIS [50] and Freiburg-Berkeley motion segmentation (FBMS) [46] benchmark datasets, and competitive results on SegTrack-v2 [38] (see §6.5). We also provide an extensive experimental analysis, with ablation studies to investigate the influence of all the components of our framework in Section 6.4.1.

Preliminary versions of this work have been published at CVPR [63] and ICCV [64]. Here, we extend these previous publications by: (i) significantly improving the performance of MP-Net with better optical flow estimation and finetuning the network on real videos (see §6.3.2 and §6.3.3), (ii) replacing the DeepLab v1 [9] appearance stream in our moving object segmentation framework with the ResNet-based DeepLab v2 [10] and showing that this indeed improves the performance (see §6.4.1), (iii) studying the effect of motion estimation quality on the overall segmentation results (see §6.4.2), and (iv) providing an analysis of the learned spatio-temporal representation (see §6.6).

Score code and trained models are available online at <http://thoth.inrialpes.fr/research/lvo>.

## 2 Related work

Our work is related to: motion and scene flow estimation, video object segmentation, and recurrent neural networks. We will review the most relevant work on these topics in the remainder of this section.

**Motion estimation.** Early attempts for estimating motion have focused on geometry-based approaches, such as [65], where the potential set of motions is identified with RANSAC. Recent methods have relied on other cues to estimate moving object regions. For example, Papzoglou and Ferrari [47] first extract motion boundaries by measuring changes in the optical flow field, and use it to estimate moving regions. They also refine this initial estimate iteratively with appearance features. This approach produces interesting results, but is limited by its heuristic initialization. We show that incorporating our learning-based motion estimation into it improves the results significantly (see Table 7).



**Fig. 2** (a,b) Two example frames from a sequence in the FlyingThings3D dataset [41]. The camera is in motion in this scene, along with four independently moving objects. (c) Ground-truth optical flow of (a), which illustrates motion of both foreground objects and background with respect to the next frame (b). (d) Ground-truth segmentation of moving objects in this scene.

Narayana et al. [43] use optical flow orientations in a probabilistic model to assign per-pixel labels that are consistent with their respective real-world motion. This approach assumes pure translational camera motion, and is prone to errors when the object and camera motions are consistent with each other. Bideau et al. [4] presented an alternative to this, where initial estimates of foreground and background motion models are updated over time, with optical flow orientations of the new frames. This initialization is also heuristic, and lacks a robust learning framework. While we also set out with the goal of finding objects in motion, our solution to this problem is a novel learning-based method. Scene flow, i.e., 3D motion field in a scene [66], is another form of motion estimation, but is computed with additional information, such as disparity values computed from stereo images [27, 69], or estimated 3D scene models [67]. None of these methods follows a CNN-based learning approach, in contrast to our method.

In concurrent work, Jain et al. [30] presented a deep network to segment independent motion in the flow field. While their approach is related to ours, they use frame pairs from real videos, in contrast to synthetic data in our case. Consequently, their work relies on estimated optical flow in training. Since obtaining accurate ground truth moving object segmentation labels is prohibitively expensive for a large dataset, they rely on an automatic, heuristic-based label estimation approach, which results in noisy annotations. We explore the pros and cons of using this realistic but noisy dataset for training our motion segmentation model in Section 6.3.3.

**Video object segmentation.** The task of segmenting objects in video is to associate pixels belonging to a class spatio-temporally; in other words, extract segments that respect object boundaries, as well as associate object pixels temporally whenever they appear in the video. This can be accomplished by propagating manual segment labels in one or more frames to the rest of the video sequence [2]. This class of methods is not applicable to our scenario, where no manual segmentation is available.

Our approach to solve the segmentation problem does not require any manually-marked regions. Several methods

in this paradigm generate an over-segmentation of videos [5, 23, 32, 37, 71]. While this can be a useful intermediate step for some recognition tasks in video, it has no notion of objects. Indeed, most of the extracted segments in this case do not directly correspond to objects, making it non-trivial to obtain video object segmentation from this intermediate result. An alternative to this is clustering pixels spatio-temporally based on motion features computed along individual point trajectories [6, 17, 45], which produces more coherent regions. They, however, assume homogeneity of motion over the entire object, which is invalid for non-rigid objects.

Another class of segmentation methods casts the problem as a foreground-background classification task [15, 36, 47, 61, 68, 72]. Some of these first estimate a region [47, 68] or regions [36, 72], which potentially correspond(s) to the foreground object, and then learn foreground/background appearance models. The learned models are then integrated with other cues, e.g., saliency maps [68], pairwise constraints [47, 72], object shape estimates [36], to compute the final object segmentation. Alternatives to this framework have used: (i) long-range interactions between distinct parts of the video to overcome noisy initializations in low-quality videos [15], and (ii) occluder/occluded relations to obtain a layered segmentation [61]. While our proposed method is similar in spirit to this class of approaches, in terms of formulating segmentation as a classification problem, we differ from previous work significantly. We propose an integrated approach to learn appearance and motion features, and update them with a memory module, in contrast to estimating an initial region heuristically and then propagating it over time. Our robust model outperforms all the top ones from this class [15, 36, 47, 61, 68], as shown in Section 6.5.

Very recently, CNN-based methods for video object segmentation were proposed [8, 30, 33]. Starting with CNNs pretrained for image segmentation, two of these methods [8, 33] find objects in video by finetuning on the first frame in the sequence. Note that this setup, referred to as semi-supervised segmentation, is very different from the more challenging unsupervised case we address in this paper, where no manually-annotated frames are available for the test video. Furthermore, these two CNN architectures are primarily developed for images, and do not model temporal information

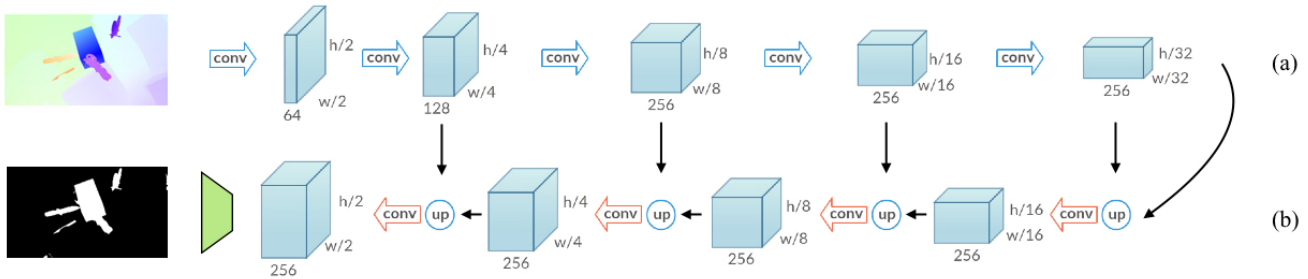


**Fig. 3** Our motion pattern network: MP-Net. The blue arrows in the encoder part (a) denote convolutional layers, together with ReLU and max-pooling layers. The red arrows in the decoder part (b) are convolutional layers with ReLU, ‘up’ denotes  $2 \times 2$  upsampling of the output of the previous unit. The unit shown in green represents bilinear interpolation of the output of the last decoder unit.

in video. We, on the other hand, propose a recurrent network specifically for the video segmentation task. Jain et al. [30] augment their motion segmentation network with an appearance model and learn the parameters of a layer to combine the predictions of the two. Their model does not feature a memory module, and also remains frame-based. Thus, it can not exploit the temporal consistency in video. We outperform [30] on DAVIS and FBMS.

**Recurrent neural networks (RNNs).** RNN [26, 55] is a popular model for tasks defined on sequential data. Its main component is an internal state that allows to accumulate information over time. The internal state in classical RNNs is updated with a weighted combination of the input and the previous state, where the weights are learned from training data for the task at hand. Long short-term memory (LSTM) [25] and GRU [11] architectures are improved variants of RNN, which partially mitigate the issue of vanishing gradients [24, 48]. They introduce gates with learnable parameters, to update the internal state selectively, and can propagate gradients further through time.

Recurrent models, originally used for text and speech recognition, e.g., [21, 42], are becoming increasingly popular for visual data. Initial work on vision tasks, such as image captioning [12], future frame prediction [59] and action recognition [44], has represented the internal state of the recurrent models as a 1D vector—without encoding any spatial information. LSTM and GRU architectures have been extended to address this issue with the introduction of ConvLSTM [16, 49, 57] and ConvGRU [3] respectively. In these convolutional recurrent models the state and the gates are 3D tensors and the weight vectors are replaced by 2D convolutions. These models have only recently been applied to vision tasks, such as video frame prediction [16, 49, 57], action recognition and video captioning [3].

In this paper, we employ a visual memory module based on a convolutional GRU (ConvGRU), and show that it is an effective way to encode the spatio-temporal evolution of objects in video for segmentation. Further, to fully benefit

from all the frames in a video sequence, we apply the recurrent model bidirectionally [20, 22], i.e., apply two identical model instances on the sequence in forward and backward directions, and combine the predictions for each frame. This makes our memory module a *bidirectional convolutional recurrent model*.

### 3 Learning to segment moving objects in videos

We start by describing the overall architecture of our video object segmentation framework. It takes video frames together with their estimated optical flow as input, and outputs binary segmentations of moving objects, as shown in Figure 1. We target the most general form of this task, wherein objects are to be segmented in the entire video if they move in at least one frame. The proposed model is comprised of three key components: appearance and motion networks, and a visual memory module described below.

**Appearance network.** The purpose of the appearance stream is to produce a high-level encoding of a frame that will later aid the visual memory module in forming a representation of the moving object. It takes a  $w \times h$  RGB frame as input and produces a  $128 \times w/8 \times h/8$  feature representation (shown in green in Figure 1), which encodes the semantic content of the scene. As a baseline for this stream we use the largeFOV, VGG16-based version of the DeepLab network [9]. This network’s architecture is based on dilated convolutions [9], which preserve a relatively high spatial resolution of features, and also incorporate context information in each pixel’s representation. It is pretrained on a semantic segmentation dataset [14], resulting in features that can distinguish objects from background as well as from each other—a crucial aspect for the video object segmentation task. We also experiment (in §6.4.1) with upgrading the appearance stream to DeepLab-v2 [10], a more recent version of the model, where the VGG16 architecture is replaced with ResNet101, and the network is additionally pretrained on the COCO semantic segmentation dataset [39].



**Motion network.** For the temporal stream we employ a CNN pretrained for the motion segmentation task. It is trained to estimate independently moving objects (i.e., irrespective of camera motion) based on optical flow computed from a pair of frames as input; see Section 4 for details. This stream (shown in yellow in Figure 1) produces a  $w/4 \times h/4$  motion prediction output, where each value represents the likelihood of the corresponding pixel being in motion. Its output is further downsampled by a factor 2 (in  $w$  and  $h$ ) to match the dimension of the appearance stream output.

The intuition behind using two streams is to benefit from their complementarity for building a strong representation of objects that evolves over time. For example, both appearance and motion networks are equally effective when an object is moving in the scene, but as soon as it becomes stationary, the motion network can not estimate the object, unlike the appearance network. We leverage this complementary nature, as done by two-stream networks for other vision tasks [58]. Note that our approach is not specific to the particular networks described above, but is in fact a general framework for video object segmentation. As shown in the Section 6.4.1, its components can easily be replaced with other networks, providing scope for future improvement.

**Memory module.** The third component, i.e., a visual memory module, takes the concatenation of appearance and motion stream outputs as its input. It refines the initial estimates from these two networks, and also memorizes the appearance and location of objects in motion to segment them in frames where: (i) they are static, or (ii) motion prediction fails. The output of this ConvGRU memory module is a  $64 \times w/8 \times h/8$  feature map obtained by combining the two-stream input with the internal state of the memory module, as described in detail in Section 5. We further improve the model by processing the video bidirectionally; see Section 5.1. The output from the ConvGRU module is processed by a  $1 \times 1$  convolutional layer and a softmax nonlinearity to produce the final pairwise segmentation result.

## 4 Motion pattern network

Our MP-Net takes the optical flow field corresponding to two consecutive frames of a video sequence as input, and produces per-pixel motion labels. We treat each video as a sequence of frame pairs, and compute the labels independently for each pair. As shown in Figure 3, the network comprises several “encoding” (convolutional and max-pooling) and “decoding” (upsampling and convolutional) layers. The motion labels are produced by the last layer of the network, which are then rescaled to the original image resolution (see §4.1). We train the network on synthetic data—a scenario where ground-truth motion labels can be acquired easily (see §4.2). We also experiment with finetuning our MP-Net on

real videos (see §6.3.3). For a detailed discussion of motion patterns our approach detects refer to §4.3.

### 4.1 Network architecture

Our encoder-decoder style network is motivated by the goal of segmenting diverse motion patterns in flow fields, which requires a large receptive field as well as an output at the original image resolution. A large receptive field is critical to incorporate context into the model. For example, when the spatial region of support (for performing convolution) provided by a small receptive field falls entirely within an object with non-zero flow values, it is impossible to determine whether it is due to object or camera motion. On the other hand, a larger receptive field will include regions corresponding to the object as well as background, providing sufficient context to determine what is moving in the scene. The second requirement of output generated at the original image resolution is to capture fine details of objects, e.g., when only a part of the object is moving. Our network satisfies these two requirements with: (i) the encoder part learning features with receptive fields of increasing sizes, and (ii) the decoder part upsampling the intermediate layer outputs to finally predict labels at the full resolution. This approach is inspired by recent advances in semantic segmentation, where similar requirements are encountered [54].

Figure 3 illustrates our network architecture. Optical flow field input is processed by the encoding part of the network (denoted by (a) in the figure) to generate a coarse representation that is a  $32 \times 32$  downsampled version of the input. Each 3D block here represents a feature map produced by a set of layers. In the encoding part, each feature map is a result of applying convolutions, followed by a ReLU non-linearity layer, and then a  $2 \times 2$  max-pooling layer. The coarse representation learned by the final set of operations in this part, i.e., the  $32 \times 32$  downsampled version, is gradually upsampled by the decoder part ((b) in the figure). In each decoder step, we first upsample the output of the previous step by  $2 \times 2$ , and concatenate it with the corresponding intermediate encoded representation, before max-pooling (illustrated with black arrows pointing down in the figure). This upsampled feature map is then processed with two convolutional layers, followed by non-linearities, to produce input for the next (higher-resolution) decoding step. The final decoder step produces a motion label map at half the original resolution. We perform a bilinear interpolation on this result to estimate labels at the original resolution.

### 4.2 Training with synthetic data

We need a large number of fully-labelled examples to train a convolutional network such as the one we propose. In our

case, this data corresponds to videos of several types of objects, captured under different conditions (e.g., moving or still camera), with their respective moving object annotations. No large dataset of real-world scenes satisfying these requirements is currently available, predominantly due to the cost of generating ground-truth annotations and flow for every frame. We adopt the popular approach of using synthetic datasets, followed in other work [13,41]. Specifically, we use the FlyingThings3D dataset [41] containing 2250 video sequences of several objects in motion, with ground-truth optical flow. We augment this dataset with ground-truth moving object labels, which are accurately estimated using the disparity values and camera parameters available in the dataset, as outlined in Section 6.1. See Figure 2(d) for an illustration.

We train the network with mini-batch SGD under several settings. The one trained with ground-truth optical flow as input shows the best performance. This is analyzed in detail in Section 6.3.1. Note that, while we use ground-truth flow for training and evaluating the network on synthetic datasets, all our results on real-world test data use only the estimated optical flow. After convergence of the training procedure, we obtain a learned model for motion patterns.

Our approach capitalizes on the recent success of CNNs for pixel-level labeling tasks, such as semantic image segmentation, which learn feature representations at multiple scales in the RGB space. The key to their top performance is the ability to capture local patterns in images. Various types of object and camera motions also produce consistent local patterns in the flow field, which our model is able to learn to recognize. This gives us a clear advantage over other pixel-level motion estimation techniques [4,43] that can not detect local patterns. Motion boundary based heuristics used in [47] can be seen as one particular type of pattern, representing independent object motion. Our model is able to learn many such patterns, which greatly improves the quality and robustness of motion estimation.

### 4.3 Detecting motion patterns

We apply our trained model on synthetic (FlyingThings3D) as well as real-world (DAVIS, FBMS, SegTrack-v2) test data. Figure 4 shows sample predictions of our model on the FlyingThings3D test set with ground-truth optical flow as input. Examples in the first two rows show that our model accurately identifies fine details in objects: thin structures even when they move subtly, such as the neck of the guitar in the top-right corner in the first row (see the subtle motion in the optical flow field (b)), fine structures like leaves in the vase, and the guitar’s headstock in the second row. Furthermore, our method successfully handles objects exhibiting highly varying motions in the second example. The third row shows a limiting case, where the receptive field of our

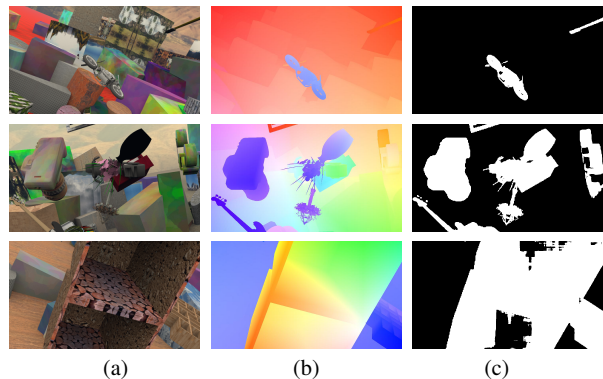


**Fig. 4** Each row shows: (a) example frame from a sequence in FlyingThings3D, (b) ground-truth optical flow of (a), which illustrates motion of both foreground objects and background, with respect to the next frame, and (c) our estimate of moving objects in this scene with ground-truth optical flow as input.

network falls entirely within the interior of a large object, as the moving object dominates. Traditional approaches, such as RANSAC, do not work in this case either.

In order to detect motion patterns in real-world videos, we first compute optical flow with popular methods [28,53,60]. With this flow as input to the network, we estimate a motion label map, as shown in the examples in Figure 5(c). Although the prediction of our frame-pair feedforward model is accurate in several regions in the frame ((c) in the figure), we are faced with two challenges, which were not observed in the synthetic training set. The first one is motion of *stuff* [1] in a scene, e.g., patterns on the water due to the kiteboarder’s motion (first row in the figure), which is irrelevant for moving object segmentation. The second one is significant errors in optical flow, e.g., in front of the pram ((b) in the bottom row in the figure). Furthermore, this motion segmentation approach is purely frame-based, thus unable to exploit temporal consistency in a video, and does not segment object in frames where they stop moving. In our previous work [63] we introduced post-processing steps to handle some of these problems. In particular, we incorporated an objectness map computed with object proposals [51] to suppress motion corresponding to stuff, as well as false positives due to errors in flow estimation. This post-processing allowed the method to achieve competitive results, but it remained frame-level. The video object segmentation framework presented in this paper addresses all these issues, as shown experimentally in Section 6.5.

## 5 ConvGRU visual memory module

The key component of the ConvGRU module is the state matrix  $h$ , which encodes the visual memory. For frame  $t$  in the video sequence, ConvGRU uses the two-stream representation  $x_t$  and the previous state  $h_{t-1}$  to compute the new

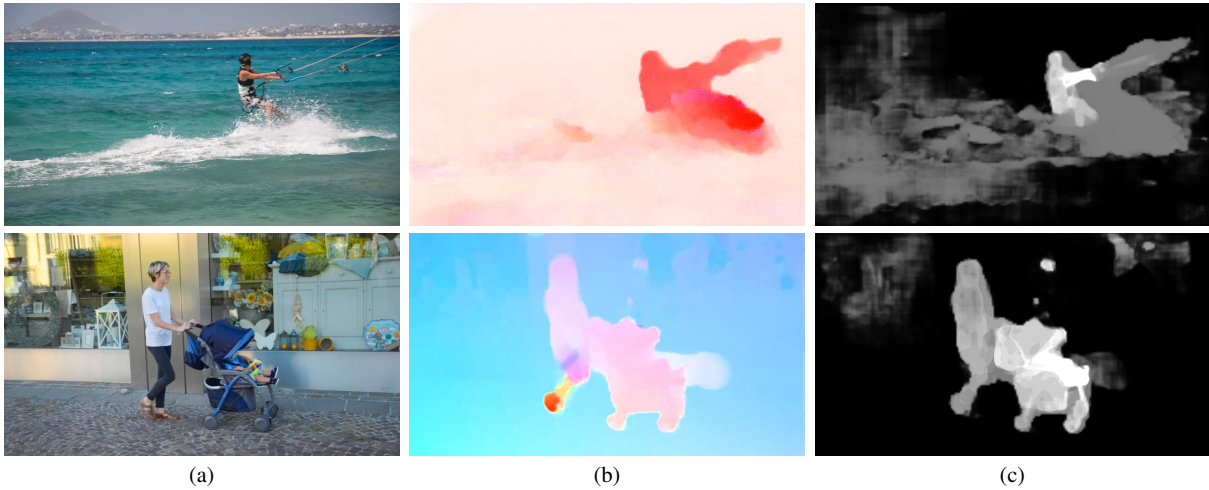


**Fig. 5** Sample results on the DAVIS dataset for MP-Net. Each row shows: (a) video frame, (b) optical flow estimated with LDOF [7], (c) output of our MP-Net with LDOF flow as input.

state  $h_t$ . The dynamics of this computation are guided by an update gate  $z_t$ , a forget gate  $r_t$ . The states and the gates are 3D tensors, and can characterize spatio-temporal patterns in the video, effectively memorizing which objects move, and where they move to. These components are computed with convolutional operators and nonlinearities as follows.

$$z_t = \sigma(x_t * w_{xz} + h_{t-1} * w_{hz} + b_z), \quad (1)$$

$$r_t = \sigma(x_t * w_{xr} + h_{t-1} * w_{hr} + b_r), \quad (2)$$

$$\tilde{h}_t = \tanh(x_t * w_{x\tilde{h}} + r_t \odot h_{t-1} * w_{h\tilde{h}} + b_{\tilde{h}}), \quad (3)$$

$$h_t = (1 - z_t) \odot h_{t-1} + z_t \odot \tilde{h}_t, \quad (4)$$

where  $\odot$  denotes element-wise multiplication,  $*$  represents a convolutional operation,  $\sigma$  is the sigmoid function,  $w$ 's are learned transformations, and  $b$ 's are bias terms.

The new state  $h_t$  in (4) is a weighted combination of the previous state  $h_{t-1}$  and the candidate memory  $\tilde{h}_t$ . The update gate  $z_t$  determines how much of this memory is incorporated into the new state. If  $z_t$  is close to zero, the memory represented by  $\tilde{h}_t$  is ignored. The reset gate  $r_t$  controls the influence of the previous state  $h_{t-1}$  on the candidate memory  $\tilde{h}_t$  in (3), i.e., how much of the previous state is let through into the candidate memory. If  $r_t$  is close to zero, the unit forgets its previously computed state  $h_{t-1}$ .

The gates and the candidate memory are computed with convolutional operations over  $x_t$  and  $h_{t-1}$  shown in equations (1-3). We illustrate the computation of the candidate memory state  $\tilde{h}_t$  in Figure 6. The state at  $t - 1$ ,  $h_{t-1}$ , is first multiplied (element-wise) with the reset gate  $r_t$ . This modulated state representation and the input  $x_t$  are then convolved with learned transformations,  $w_{h\tilde{h}}$  and  $w_{x\tilde{h}}$  respectively, summed together with a bias term  $b_{\tilde{h}}$ , and passed through a tanh nonlinearity. In other words, the visual memory representation of a pixel is determined not only by the input and the previous state at that pixel, but also its local neighborhood. Increasing the size of the convolutional

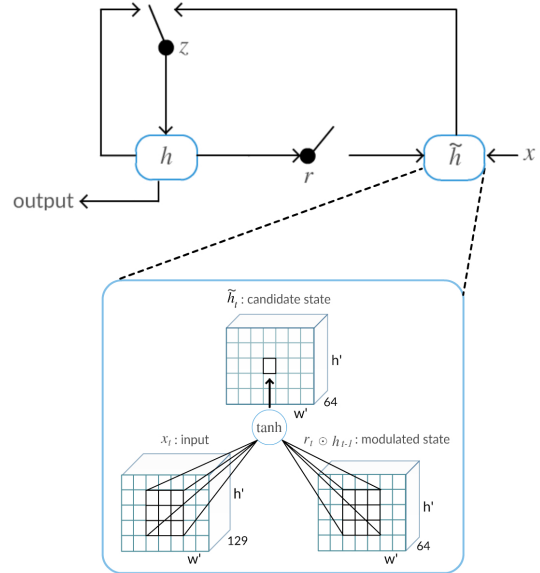


**Fig. 6** Illustration of ConvGRU with details for the candidate hidden state module, where  $\tilde{h}_t$  is computed with two convolutional operations and a tanh nonlinearity.

kernels allows the model to handle spatio-temporal patterns with larger motion.

The update and reset gates,  $z_t$  and  $r_t$ , are computed in an analogous fashion using a sigmoid function instead of tanh. Our ConvGRU applies a total of six convolutional operations at each time step. All the operations detailed here are fully differentiable, and thus the parameters of the convolutions ( $w$ 's and  $b$ 's) can be learned in an end-to-end fashion with back propagation through time [70]. In summary, the model learns to combine appearance features of the current frame with the memorized video representation to refine motion predictions, or even fully restore them from the

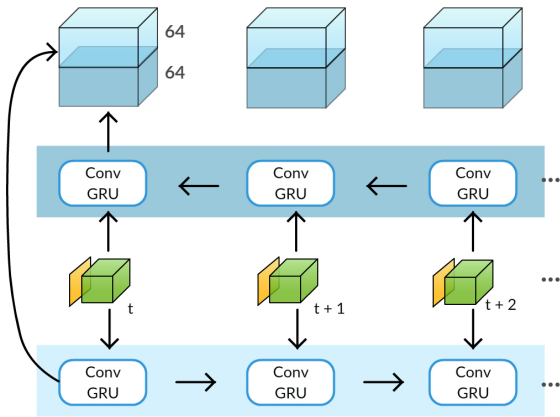


**Fig. 7** Illustration of the bidirectional processing with our ConvGRU module.

previous observations in case a moving object becomes stationary.

### 5.1 Bidirectional processing

Consider an example where an object is stationary at the beginning of a video sequence, and starts to move in the latter frames. Our approach described so far, which processes video frames sequentially (in the forward direction), starting with the first frame can not segment the object in the initial frames. This is due to the lack of prior memory representation of the object in the first frame. We improve our framework with a bidirectional processing step, inspired by the application of recurrent models bidirectionally in the speech domain [20, 22].

The bidirectional variant of our ConvGRU is illustrated in Figure 7. It is composed of two ConvGRU instances with identical learned weights, which are run in parallel. The first one processes frames in the forward direction, starting with the first frame (shown at the bottom in the figure). The second instance process frames in the backward direction, starting with the last video frame (shown at the top in the figure). The activations from these two directions are concatenated at each time step, as shown in the figure, to produce a  $128 \times w/8 \times h/8$  output. It is then passed through a  $3 \times 3$  convolutional layer to finally produce a  $64 \times w/8 \times h/8$  output for each frame. Pixel-wise segmentation from this activation is the result of the last  $1 \times 1$  convolutional layer and softmax nonlinearity, as in the unidirectional case.

Bidirectional ConvGRU is used both in training and in testing, allowing the model to learn to aggregate information over the entire video. In addition to handling cases where objects move in the latter frames, it improves the ability of the model to correct motion prediction errors. As discussed in the experimental evaluation, bidirectional ConvGRU improves segmentation performance by nearly 3% on

the DAVIS dataset (see Table 4). The influence of bidirectional processing is more prominent on the FBMS dataset, where objects can be static in the beginning of a video, with 5% improvement over the unidirectional variant.

### 5.2 Training

We train our visual memory module with the back propagation through time algorithm [70], which unrolls the recurrent network for  $n$  time steps and keeps all the intermediate activations to compute the gradients. Thus, our ConvGRU model, which has six internal convolutional layers, trained on a video sequence of length  $n$ , is equivalent to a  $6n$  layer CNN for the unidirectional variant, or  $12n$  for the bidirectional model at training time. This memory requirement makes it infeasible to train the whole model, including appearance and motion streams, end-to-end. We resort to using pretrained versions of the appearance and motion networks, and train the ConvGRU.

In contrast to our motion segmentation model, which is learned on synthetic videos, we use the training split of the DAVIS dataset [50] for learning the ConvGRU weights. Despite being an order of magnitude smaller, DAVIS consists of realistic videos, which turns out to be crucial for effective use of appearance stream to correct motion estimation errors (see §6.4.1). Since objects move in all the frames in DAVIS, it biases the memory module towards the presence of an uninterrupted motion stream. This results in the ConvGRU learned from this data failing, when an object stops to move in a test sequence. We augment the training data to simulate such *stop-and-go* scenarios to learn a more robust model for realistic videos. To this end, we create additional sequences where we duplicate the last frame five times, i.e., we create a part of the video in which the object is static. This setting allows ConvGRU to learn how to segment objects even if they are static, i.e., it explicitly memorize the moving object in the initial part of the sequence, and then segments it in frames where the motion stops. We also augment the training data by duplicating the first five frames to simulate scenarios where the object is static in the beginning of a sequence.

## 6 Experiments

### 6.1 Datasets and evaluation

We use five datasets in the experimental analysis: FT3D and DAVIS for training and test, FusionSeg only for training, and FBMS and SegTrack-v2 only for test.

**FlyingThings3D (FT3D).** We train our motion segmentation network with the synthetic FlyingThings3D dataset [41].



It contains videos of various objects flying along randomized trajectories, in randomly constructed scenes. The video sequences are generated with complex camera motion, which is also randomized. FT3D comprises 2700 videos, each containing 10 stereo frames. The dataset is split into training and test sets, with 2250 and 450 videos respectively. Ground-truth optical flow, disparity, intrinsic and extrinsic camera parameters, and object instance segmentation masks are provided for all the videos. No annotation is directly available to distinguish moving objects from stationary ones, which is required to train our network. We extract this from the data provided as follows. With the given camera parameters and the stereo image pair, we first compute the 3D coordinates of all the pixels in a video frame  $t$ . Using ground-truth flow between frames  $t$  and  $t + 1$  to find a pair of corresponding pixels, we retrieve their respective 3D scene points. Now, if the pixel has not undergone any independent motion between these two frames, the scene coordinates will be identical (up to small rounding errors). We have made these labels publicly available on our project website<sup>1</sup>. Performance on the test set is measured as the standard intersection over union score between the predicted segmentation and the ground-truth masks.

**DAVIS.** We use the densely annotated video segmentation dataset [50] for evaluation as well as for training our visual memory module. DAVIS contains 50 full HD videos, featuring diverse types of object and camera motion. It includes challenging examples with occlusion, motion blur and appearance changes. Accurate pixel-level annotations are provided for the moving object in all the video frames. A single object is annotated in each video, even if there are multiple moving objects in the scene. Following the 30/20 training/validation split provided with the dataset, we train the visual memory module on the 30 sequences, and test on the 20 validation videos. Note that our motion segmentation model is also evaluated separately on the entire trainval set, as it is trained exclusively on FT3D. We evaluate on DAVIS with the three measures used in [50], namely intersection over union for region similarity, F-measure for contour accuracy, and temporal stability for measuring the smoothness of segmentation over time. We follow the protocol in [50] and use images downsampled by a factor of two.

**FusionSeg.** Jain et al. [30] recently introduced a dataset containing 84929 pairs of frames extracted from the ImageNet-Video dataset [56]. The frames are annotated with an automatic segmentation method, which combines a foreground-background appearance-based model with ground truth bounding box annotations available in ImageNet-Video. Annotations obtained in this way may be inaccurate, but are useful for analyzing the impact of learning the motion network on

these realistic examples, in contrast to using synthetic examples; see Section 6.3.3. We will refer to this dataset as FusionSeg in the rest of the paper.

**FBMS.** The Freiburg-Berkeley motion segmentation dataset [46] is composed of 59 videos with ground truth annotations in a subset of frames. In contrast to DAVIS, it has multiple moving objects in several videos with instance-level annotations. Also, objects may move only in a fraction of the frames, but are annotated in frames where they do not exhibit independent motion. The dataset is split into training and test set. Following the standard protocol on this dataset [31], we do not train on any of these sequences, and evaluate separately on both splits with precision, recall and F-measure scores. We also convert instance-level annotation to binary ones by merging all the foreground labels into a single category, as in [61].

**SegTrack-v2.** It contains 14 videos with instance-level moving object annotations in all the frames. We convert these annotations into a binary form for evaluation and use intersection over union as the performance measure. Note that some videos in this dataset are of very low resolution, which appears to have a negative effect on the performance of deep learning-based methods trained on high resolution images.

## 6.2 Implementation details

*Appearance stream.* For the experiments using DeepLab-v1, we extract features from the fc6 layer of the network, which has a dilation of 12. This approach cannot be followed for DeepLab-v2 however, since dilation is applied to fc8, the prediction layer, in this improved model. Thus, extracting fc6 or fc7 features of DeepLab-v2 would result in a decreased field of view compared to the baseline v1 model. Moreover, there are four independent prediction layers in v2 with dilations 6, 12, 18 and 24, whose outputs are averaged. To make the feature representation derived from the two architectures compatible, we introduce four new penultimate convolutional layers to the DeepLab-v2 architecture. These layers have kernel size 3, feature dimension 512 and dilations corresponding to those in the prediction layers of DeepLab-v2. The maximum response over these four feature maps is then passed to a single prediction layer. We fine-tune this model on PASCAL VOC 2012 for semantic segmentation. The features after the max operation are used as the appearance representation in our final model, and correspond to an improved version of fc6 features from DeepLab-v1. This representation is further passed through two  $1 \times 1$  convolutional layers, interleaved with *tanh* nonlinearities, to reduce the dimension to 128 for both architectures.

<sup>1</sup> <http://thoth.inrialpes.fr/research/mpnet>

*Training MP-Net.* We use mini-batch SGD with a batch size of 13 images—the maximum possible due to GPU memory constraints. The network is trained from scratch with learning rate set to 0.003, momentum to 0.9, and weight decay to 0.005. Training is done for 27 epochs, and the learning rate and weight decay are decreased by a factor of 0.1 after every 9 epochs. We downsample the original frames of the FT3D training set by a factor 2, and perform data augmentation by random cropping and mirroring. Batch normalization [29] is applied to all the convolutional layers of the network.

*Training visual memory module.* We minimize the binary cross-entropy loss using back-propagation through time and RMSProp [62] with a learning rate of  $10^{-4}$ . The learning rate is gradually decreased after every epoch. Weight decay is set to 0.005. Initialization of all the convolutional layers, except for those inside the ConvGRU, is done with the standard *xavier* method [18]. We clip the gradients to the  $[-50, 50]$  range before each parameter update, to avoid numerical issues [19]. We form batches of size 14 by randomly selecting a video, and a subset of 14 consecutive frames in it. Random cropping and flipping of the sequences is also performed for data augmentation. Our full model uses  $7 \times 7$  convolutions in all the ConvGRU operations. The weights of the two  $1 \times 1$  convolutional (dimensionality reduction) layers in the appearance network and the final  $1 \times 1$  convolutional layer following the memory module are learned jointly with the memory module. The model is trained for 30000 iterations and the proportion of batches with simulated motion discontinuities (see Section 5.2) is set to 20%.

*Other details.* We perform zero-mean normalization of the flow field vectors, similar to [58]. When using flow angle and magnitude together (which we refer to as flow angle field), we scale the magnitude component, to bring the two channels to the same range. Our final model uses a fully-connected CRF [35] to refine boundaries in a post-processing step. The parameters of this CRF are set to values used for a related pixel-level segmentation task [9]. Many sequences in FBMS are several hundred frames long and do not fit into GPU memory during evaluation. We apply our method in a sliding window fashion in such cases, with a window of 130 frames and a step size of 50. Our model is implemented in the Torch framework.

### 6.3 Motion pattern network

We first analyze the different design choices in our MP-Net, and then study the influence of training data and optical flow representation on the motion prediction performance.

# dec.	Trained on FT3D with ...	FT3D	DAVIS
1	RGB single frame	68.1	12.7
	RGB pair	69.1	16.6
	GT flow	74.5	44.3
	GT angle field	73.1	46.6
	RGB + GT angle field	74.8	39.6
	LDOF angle field	63.2	38.1
4	GT angle field	85.9	52.4

**Table 1** Comparing the influence of different input modalities on the FlyingThings3D (FT3D) test set and DAVIS. Performance is shown as mean intersection over union scores. # dec. refers to the number of decoder units in our MP-Net. Ground-truth flow is used for evaluation on FT3D and LDOF flow for DAVIS.

#### 6.3.1 Influence of input modalities

We analyze the influence of different input modalities, such as RGB data (single frame and image pair), optical flow field (ground truth and estimated one) directly as flow vectors, i.e., flow in x and y axes, or as angle field (flow vector angle concatenated with flow magnitude), and a combination of RGB data and flow, on training MP-Net. These results are presented on the FT3D test set and also on DAVIS, to study how well the observations on synthetic videos transfer to the real-world ones, in Table 1. For computational reasons we train and test with different modalities on a smaller version of our MP-Net, with one decoder unit instead of four. Then we pick the best modality to train and test the full, deeper version of the network.

From Table 1, the performance on DAVIS is lower than on FT3D. This is expected as there is a domain change from synthetic to real data, and that we use ground truth optical flow as input for FT3D test data, but estimated flow [7, 60] for DAVIS. As a baseline, we train on single RGB frames (‘RGB single frame’ in the table). Clearly, no motion patterns can be learned in this case, but the network performs reasonably on FT3D test (68.1), as it learns to correlate object appearance with its motion. This intuition is confirmed by the fact that ‘RGB single frame’ fails on DAVIS (12.7), where the appearance of objects and background is significantly different from FT3D. MP-Net trained on ‘RGB pair’, i.e., RGB data of two consecutive frames concatenated, performs slightly better on both FT3D (69.1) and DAVIS (16.6), suggesting that it captures some motion-like information, but continues to rely on appearance, as it does not transfer well to DAVIS.

Training on ground-truth flow vectors corresponding to the image pair (‘GT flow’) improves the performance on FT3D by 5.4% and on DAVIS significantly (27.7%). This shows that MP-Net learned on flow from synthetic examples can be transferred to real-world videos. We then experiment with flow angle as part of the input. As discussed in [43], flow orientations are independent of depth from the camera, unlike flow vectors, when the camera is undergoing

Flow in test	FT3D	DAVIS
LDOF [60]	58.7	52.4
EpicFlow [53]	52.5	56.9
FlowNet 2.0 [28]	66.3	62.6

**Table 2** Performance of the best MP-Net variant (4 decoder units trained on GT angle field) with different flow inputs (LDOF, EpicFlow, FlowNet 2.0) on FT3D and DAVIS.

only translational motion. Using the ground truth flow angle field (concatenation of flow angles and magnitudes) as input (‘GT angle field’), we note a slight decrease in IoU score on FT3D (1.4%), where strong camera rotations are abundant, but in real examples, such motion is usually mild. Hence, ‘GT angle field’ improves IoU on DAVIS by 2.3%. We use angle field representation in all further experiments.

Using a concatenated flow and RGB representation (‘RGB + GT angle field’) performs better on FT3D (by 1.7%), but is poorer by 7% on DAVIS, re-confirming our observation that appearance features are not consistent between the two datasets. Finally, training on computed flow [7] (‘LDOF angle field’) leads to significant drop on both the datasets: 9.9% on FT3D (with GT flow for testing) and 8.5% on DAVIS, showing the importance of high-quality training data for learning accurate models. The full version of our MP-Net, with 4 decoder units, improves the IoU by 12.8% on FT3D and 5.8% on DAVIS over its shallower one-unit equivalent.

Notice that the performance of our full model on FT3D is excellent, with the remaining errors mostly due to inherently ambiguous cases like objects moving close to the camera (see third row in Figure 4), or very strong object/camera motion. On DAVIS, the results are considerably lower despite less challenging motion. To investigate the extent to which this is due to errors in flow, we study the effect of flow quality in the following section.

### 6.3.2 Effect of the flow quality

We evaluate the performance of MP-Net using two recent flow estimation methods, EpicFlow [53] and FlowNet 2.0 [28], and LDOF [7, 60], a more classical approach, on the FT3D test and DAVIS datasets in Table 2. We observe a significant drop in performance of 27.2% (from 85.9% to 58.7%) on FT3D when using LDOF, compared to evaluation with the ground truth in Table 1. This confirms the impact of optical flow quality and suggests that improvements in flow estimation can increase the performance of our method on real-world videos, where no ground truth flow is available.

We experimentally demonstrate this improvement, by utilizing state-of-the-art flow estimation methods, instead of LDOF. EpicFlow, which leverages motion contours, produces more accurate object boundaries, and improves over MP-Net using LDOF by 4.5% on DAVIS. On FT3D though it leads to a 6.2% decrease in performance. We observe that

Trained on	FT3D	DAVIS
FT3D	85.9	62.6
FusionSeg	40.8	60.4
FT3D + FusionSeg	43.0	63.9
DAVIS	34.0	62.3
FT3D + DAVIS	45.7	66.7
FT3D + FusionSeg + DAVIS	40.8	68.6

**Table 3** Performance of the best MP-Net variant trained with different datasets on FT3D test and DAVIS validation sets. FlowNet 2.0 is used for flow estimation on DAVIS both in training and in testing in all these experiments.

this is due to EpicFlow, which does produce more accurate object boundaries, but also smooths out small objects and objects with tiny motions. This smoothing appears to be beneficial on real videos, but degrades the performance on synthetic FT3D videos. FlowNet 2.0, which is a CNN-based method trained on a mixture of synthetic and real videos to estimate optical flow from a pair of frames, further improves the performance on DAVIS by 5.7%. It also achieves better results on FT3D, with a 7.6% improvement over LDOF. The remaining gap of 19.6% between the ground truth flow and FlowNet 2.0 performance on FT3D shows the potential for future improvement of flow estimation methods.

### 6.3.3 Training on real videos

We also experiment with training our MP-Net on FusionSeg and DAVIS, in order to explore the value real videos can bring in learning a motion segmentation model, compared to training exclusively on synthetic videos. On one hand, real videos contain motion patterns that have similar statistics to those encountered in the testing phase. On the other hand, no ground truth flow is available, so a noisy flow estimation has to be used, which was shown to be suboptimal when training on FT3D (see §6.3.1). For FusionSeg the labels are, furthermore, not ground truth, but are instead obtained automatically and contain a significant amount of noise, as discussed in §6.1.

All the models in this experiment are trained on flow extracted with the state-of-the-art FlowNet 2.0, in order to minimize the influence of errors in flow. FlowNet 2.0 is also used for evaluation on the DAVIS validation set, whereas ground truth flow is used for FT3D test set. As shown in Table 3, the model trained on FusionSeg is 2.2% below the one trained on synthetic data in the case of DAVIS. On FT3D, its performance drops by 45.1%. This shows that the synthetic dataset contains a lot more challenging motions than those typically encountered in real videos, and although a model learned on synthetic data can generalize to real data, the converse does not hold. Learning the model only on real videos also does not bring any improvement on DAVIS, due to errors in flow estimation and labels in FusionSeg outweigh

Aspect	Variant	Mean IoU
Ours (fc6, ConvGRU, Bidir, DAVIS)		70.1
App stream	no	43.5
	RGB	58.3
	2-layer CNN	60.9
	DeepLab fc7	69.8
	DeepLab conv5	67.7
	DeepLab-v2	72.5
App pretrain	ImageNet only	64.1
Motion stream	no	59.6
Memory module	no	64.1
	ConvRNN	68.7
	ConvLSTM	68.9
Bidir processing	no	67.2
Train data	FT3D GT Flow	55.3
	FT3D LDOF Flow	59.6

**Table 4** Ablation study on the DAVIS validation set showing variants of appearance and motion streams and memory module. “Ours” refers to the model using fc6 appearance features together with a motion stream, and a bidirectional ConvGRU trained on DAVIS.

ing the potential benefits. We then finetune the FT3D-trained model on FusionSeg to leverage the benefits of the two domains. This leads to a notable improvement on both datasets, e.g., 3.5% on DAVIS compared to the model trained on FusionSeg alone. The results on synthetic FT3D videos, despite the improvement over the FusionSeg-trained model, remain low however, showing the significant difference between the two domains.

To further explore the use of real videos, we train our motion estimation model on the DAVIS training set. This dataset contains only 2079 frames, compared to 84929 in FusionSeg, but they are manually annotated, removing one source of errors due to incorrect labels from training. The performance on DAVIS increases by 1.9% with this, compared to training on FusionSeg. On FT3D, though, IoU decreases by 6.8%, because the variety of motions in DAVIS is even smaller than that seen in FusionSeg. Combining the synthetic and real datasets, i.e., training on FT3D and finetuning on DAVIS, improves the performance on both FT3D and DAVIS. Finetuning the FT3D-trained model with FusionSeg and then DAVIS training data further improves the performance on the DAVIS validation set, but results in a drop in the case of FT3D, as the model is even more different from synthetic data.

## 6.4 Video object segmentation framework

### 6.4.1 Ablation study

Table 4 demonstrates the influence of different components of our approach on the DAVIS validation set. We use the model with DeepLab-v1 appearance stream, ConvGRU memory module, bi-directional processing, motion network trained

on FT3D+GT-flow and LDOF used for flow estimation on DAVIS as a baseline. We learn all the models on the training set of DAVIS. First, we study the role of the appearance stream. As a baseline, we remove it completely (“no” in “App stream” in the table), i.e., the output of the motion stream is the only input to our visual memory module. In this setting, the memory module lacks sufficient information to produce accurate segmentations, which results in an 26.6% drop in performance compared to the method where the appearance stream with fc6 features is used (“Ours” in the table). We then provide raw RGB frames, concatenated with the motion prediction, as input to the ConvGRU. This simplest form of image representation leads to a 14.8% improvement, compared to the motion only model, showing the importance of the appearance features. The variant where RGB input is passed through two convolutional layers, interleaved with tanh nonlinearities, that are trained jointly with the memory module (“2-layer CNN”), further improves this. This shows the potential of learning appearance representation as a part of the video segmentation pipeline. Next, we compare features extracted from the fc7 and conv5 layers of the DeepLab model to those from fc6 used by default in our method. Features from fc7 and fc6 show comparable performance, but fc7 ones are more expensive to compute. Conv5 features perform significantly worse, perhaps due to a smaller field of view. Finally, we replace the VGG16-based DeepLab architecture with the ResNet101-based DeepLab-v2, as described in Section 3. This improves the performance over DeepLab-v1 by 2.4%, which is consistent with our previous observations that better representations directly affect the overall performance of the method. We thus use DeepLab-v2 appearance stream in our final model.

The importance of appearance network pretrained on the semantic segmentation task is highlighted by the “ImageNet only” variant in Table 4, where the PASCAL VOC pretrained DeepLab segmentation network is replaced with a network trained on ImageNet classification. Although ImageNet pre-training provides a rich feature representation, it is less suitable for the video object segmentation task, which is confirmed by an 6% drop in performance. Surprisingly, the variant of our approach that discards the motion information (“no” in “Motion stream”), although being 10.5% below the baseline, still outperforms many of the state-of-the-art methods on DAVIS (see Table 6). This variant learns foreground/background segmentation, which is sufficient for videos with a single dominant object, but fails in more challenging cases. Section 6.4.2 presents additional experiments to explore the quality of motion estimation during the training and testing phases.

Next, we evaluate the design choices in the visual memory module. We replaced the memory module (ConvGRU) with a stack of six convolutional layers to obtain ‘no memory’ variant of our model (“no” in “Memory module” in Table 4), but with the same number of parameters. This vari-



ant results in a 6% drop in performance compared to our full model with ConvGRU on the DAVIS validation set. The performance of the ‘no memory’ variant is comparable to 63.3, the performance of “MP-Net+Obj,” the approach without any memory (see Table 2 in [63]). Using a simple recurrent model (ConvRNN) results in a slight decrease in performance. Such simpler architectures can be used in case of a memory vs segmentation quality trade off. The other variant using ConvLSTM is comparable to ConvRNN, possibly due to the lack of sufficient training data. Performing unidirectional processing instead of a bidirectional one decreases the performance by nearly 3% (“no” in “Bidir processing”).

Lastly, we train two variants (“FT3D GT Flow” and “FT3D LDOF Flow”) on the synthetic FT3D dataset [41] instead of DAVIS. Both of them show a significantly lower performance than our method trained on DAVIS. This is due to the appearance of synthetic FT3D videos being very different from the real-world ones. The variant trained on ground truth flow (GT Flow) is inferior to that trained on LDOF flow because the motion network (MP-Net) achieves a high performance on FT3D with ground truth flow, and thus our visual memory module learns to simply follow the motion stream output.

#### 6.4.2 Influence of the motion network

In Sections 6.3.2 and 6.3.3 we have demonstrated that the performance of MP-Net can be improved by using more accurate optical flow estimation methods, and finetuning the network on FusionSeg and DAVIS. Here we explore the influence of these improvements in motion estimation on our video object segmentation framework. In Table 5 we evaluate the best version of our framework so far (DeepLab-v2 appearance stream, ConvGRU memory module trained on DAVIS, Bi-directional processing) with baseline and improved versions of MP-Net. The version denoted as ‘FT3D + LDOF’ in the table corresponds to the segmentation model with baseline MP-Net (trained on FT3D only), and LDOF used for flow estimation on DAVIS, whereas ‘FSeg + FNet’ corresponds to the model with improved MP-Net (finetuned on FusionSeg) and FlowNet 2.0 used for flow estimation. Note that the variant of MP-Net finetuned on FusionSeg and then on DAVIS, which showed the best results in the Section 6.3.3, leads to a drop in performance of our video segmentation framework when used in training due to overfitting on the small number of sequences in DAVIS, thus we do not include it in the comparison. We independently evaluate the effect of replacing the baseline MP-Net with the improved one in training and testing on DAVIS.

The main observation from the results in Table 5 is that our approach is fairly robust to the motion estimation model being used. The performance differs by at most 3% here, whereas the MP-Net variants differ by 11.5%, as seen in Ta-

Train	Test	Mean IoU	+ CRF
FT3D + LDOF	FT3D + LDOF	72.5	76.8
FT3D + LDOF	FSeg + FNet	72.0	75.3
FSeg + FNet	FSeg + FNet	73.3	78.2
FSeg + FNet	FT3D + LDOF	70.2	76.2

**Table 5** Influence of motion stream variants, used in training and test phases on DAVIS. ‘FT3D + LDOF’ corresponds to the segmentation model with baseline MP-Net (trained on FT3D only), and LDOF used for flow estimation on DAVIS. ‘FSeg + FNet’ is the variant with improved MP-Net (finetuned on FusionSeg), and FlowNet 2.0 used for flow estimation.

bles 2 and 3. This shows that the visual memory module learns to use appearance and temporal consistency cues to overcome variations in quality of motion estimation.

The performance on the DAVIS validation set is best when the same motion model is used in the training and the test phases; see the second and the third rows in Table 5 for a comparison. This is expected because ConvGRU adapts to the motion model used in training, and suffers from a domain shift problem, if this model is replaced during the test phase. The variant trained and tested with the ‘FSeg + FNet’ model (row 3 in the table), which shows the best performance, with or without the CRF post-processing is used in the final version of the model.

#### 6.5 Comparison to the state-of-the-art

In this section we compare the best version of our method (DeepLab-v2 appearance stream, ConvGRU memory module trained on DAVIS, Bi-directional processing, MP-Net finetuned on FusionSeg with FlowNet 2.0 used or flow estimation (FSeg + FNet) and DenseCRF [35] post-processing) to the state-of-the-art methods on 3 benchmark datasets: DAVIS, FBMS and SegTrack-v2.

**DAVIS.** Table 6 compares our approach to the state-of-the-art methods on DAVIS. In addition to comparing our results to the top-performing unsupervised approaches reported in [50], we included the results of recent methods from the benchmark website:<sup>2</sup> CUT [31], FSG [30] and ARP [34], as well as the frame-level variant of our method: MP-Net-F [63]. This frame-level approach augments our motion estimation model with an heuristic-based objectness score and uses DenseCRF for postprocessing (boundary refinement). Our method outperforms ARP [34], the previous state of the art by 2% on the mean IoU measure. We also observe an 8.2% improvement over MP-Net-F in mean IoU and 36.1% in temporal stability, which clearly demonstrates the significance of the visual memory module.

<sup>2</sup> [http://davischallenge.org/soa\\_compare.html](http://davischallenge.org/soa_compare.html)

Measure		CVOS [61]	KEY [36]	MSG [6]	NLC [15]	CUT [31]	FST [47]	MP-Net-F [63]	FSG [30]	ARP [34]	Ours
$\mathcal{J}$	Mean	48.2	49.8	53.3	55.1	55.2	55.8	70.0	70.7	76.2	78.2
	Recall	54.0	59.1	61.6	55.8	57.5	64.9	85.0	83.5	91.1	89.1
	Decay	10.5	14.1	2.4	12.6	2.3	0.0	1.4	1.5	7.0	4.1
$\mathcal{F}$	Mean	44.7	42.7	50.8	52.3	55.2	51.1	65.9	65.3	70.6	75.9
	Recall	52.6	37.5	60.0	51.9	61.0	51.6	79.2	73.8	83.5	84.7
	Decay	11.7	10.6	5.1	11.4	3.4	2.9	2.5	1.8	7.9	3.5
$\mathcal{T}$	Mean	24.4	25.2	29.1	41.4	26.3	34.3	56.3	32.8	39.3	20.2

**Table 6** Comparison to the state-of-the-art methods on DAVIS with intersection over union ( $\mathcal{J}$ ), F-measure ( $\mathcal{F}$ ), and temporal stability ( $\mathcal{T}$ ).



**Fig. 8** Qualitative comparison with the top-performing methods on DAVIS. Left to right: ground truth, results of MP-Net-F [63], FSG [30], ARP [34], and our method.

Figure 8 shows qualitative results of our approach, and the next three top-performing methods on DAVIS: MP-Net-F [63], FSG [30] and ARP [34]. In the first row, our method fully segments the dancer, whereas MP-Net-F and FSG miss various parts of the person and ARP segments some of the people in the background. All these approaches use heuristics to combine motion and appearance cues, which become unreliable in cluttered scenes with many objects. Our approach does not include any heuristics, which makes it robust to this type of errors. In the second row, all the methods segment the car, but only our approach does not leak into other cars in the video, showing high discriminability. In the next row, our approach is able to fully segment a complex object, whereas the other methods either miss parts of it (MP-Net-F and FSG) or segment background regions as moving (ARP). In the last row, we illustrate a failure case of our method. The people in the background move in some of the frames in this example. MP-Net-F, FSG and our method segment them to varying extents. ARP focuses on the foreground object, but misses a part of it.

**FBMS.** As shown in Table 7, MP-Net-F [63] is outperformed by most of the methods on this dataset. Our approach based on visual memory outperforms MP-Net-F by 21.3% on the test set and by 21.0% on the training set according to the F-measure. FST [47] based post-processing (“MP-Net-V” in the table) significantly improves the results of MP-Net-F on FBMS, but it remains below our approach for all measures. We compare with ARP [34] using masks provided by the authors on the test set. Our method outperforms ARP on this set by 12.2% on the F-measure. Overall, our method shows a significantly better performance than all the other approaches in terms of precision, recall and F-measure. This demonstrates that the visual memory module, in combination with a strong appearance representation, handles complex video segmentation scenarios, where objects move only in a fraction of the frames.

Figure 9 shows qualitative results of our method and the two next-best methods on FBMS: MP-Net-V [63] and CUT [31]. MP-Net-V relies highly on FST’s [47] tracking capabilities, and thus leaks to background in the top three

Measure	Set	KEY [36]	MP-Net-F [63]	FST [47]	ARP [34]	CVOS [61]	CUT [31]	MP-Net-V [63]	Ours
$\mathcal{P}$	Training	64.9	83.0	71.3	-	79.2	86.6	69.3	89.9
	Test	62.3	84.0	76.3	76.1	83.4	83.1	81.4	93.8
$\mathcal{R}$	Training	52.7	54.2	70.6	-	79.0	80.3	80.8	83.5
	Test	56.0	49.4	63.3	66.9	67.9	71.5	73.9	75.3
$\mathcal{F}$	Training	58.2	65.6	71.0	-	79.3	83.4	74.6	86.6
	Test	59.0	62.2	69.2	71.3	74.9	76.8	77.5	83.5

**Table 7** Comparison to the state-of-the-art methods on FBMS with precision ( $\mathcal{P}$ ), recall ( $\mathcal{R}$ ), and F-measure ( $\mathcal{F}$ ).

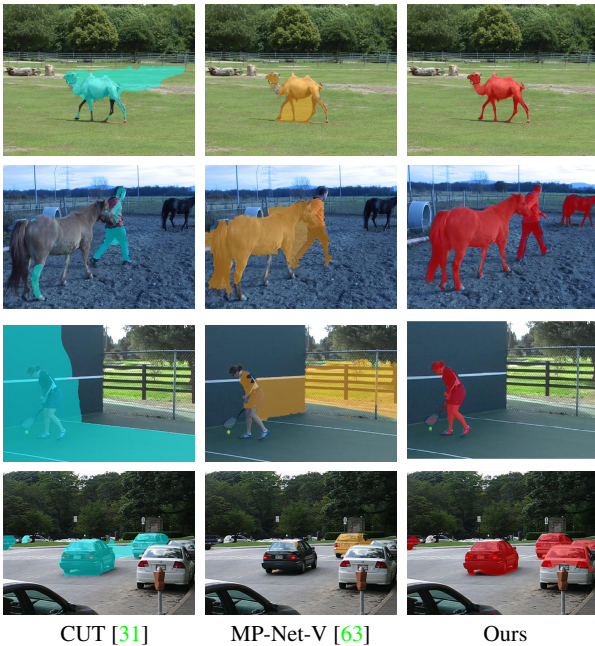


**Fig. 9** Qualitative comparison with the top-performing methods on FBMS. Left to right: results of CUT [31], MP-Net-Video [63], and our method.

examples, which is a common failure mode of FST. CUT misses parts of objects and incorrectly assigns background regions to the foreground in some cases, whereas our method demonstrates very high precision. It is also the only approach which is able to correctly segment all three moving objects in the second example. In the last row we show a failure case of our method. Although it does segment the three moving cars in this video, segmentation leaks to the static cars on the right. Our memory module uses a high-level semantic encoding of the frames to propagate noisy motion segmentations, which leads to incorrectly propagating the segmentation from the moving car to the static ones which are adjacent to it in this case. CUT also captures the three moving cars in this video, but leaks to the background. MP-Net-V does not segment static regions, but misses two of the cars.

**SegTrack-v2.** The performance of our method on SegTrack is presented in the Table 8. NLC [15] is the top-performing method, followed by FSG [30], on this dataset. Note however, that these methods are both tuned to SegTrack. FSG

Method	Mean IoU
CUT [31]	47.8
FST [47]	54.3
FSG [30]	61.4
NLC [15]	67.2
Ours	53.7
Ours w/o CRF	59.1

**Table 8** Comparison to the state-of-the-art methods on SegTrack-v2 with mean IoU.

is trained directly on a subset of SegTrack sequences, and the parameters of NLC are set manually for this dataset. In contrast, we use the same model trained on DAVIS in all the experiments, which is a possible explanation for a lower performance than NLC and FSG. As shown recently [30, 33], the low resolution of some of the SegTrack videos poses a significant challenge for deep learning-based video segmentation methods. Being trained on datasets like PASCAL VOC or COCO, which are composed of high-quality images, these models suffer from the well-known domain shift problem, when applied to low-resolution videos. Our method, with its appearance stream trained on VOC, is subject to this issue as well. Additionally, CRF post-processing decreases the performance of our method on SegTrack; see ‘Ours w/o CRF’ in Table 8 and qualitative comparison in the next paragraph.

A qualitative comparison of our method and the variant without CRF post-processing (‘Ours w/o CRF’) with NLC is presented in Figure 10. In the first row, all the three approaches are segment the moving cars in the challenging racing scene, but NLC is less precise than the two variants of our method. In the second example, the monkey is fully extracted by NLC only. Our method’s prediction (w/o CRF) is not confident due to the low resolution of the video. It is thus merged into the background by CRF refinement. In the last row, none of the methods captures the group of penguins. Our results are further diminished by the CRF, due to unreliability of the initial prediction (w/o CRF).

## 6.6 ConvGRU visualization

We present a visualization of the gate activity in our ConvGRU unit on two videos from the DAVIS validation set.





**Fig. 11** Visualization of the ConvGRU gate activations for two sequences from the DAVIS validation set. The first row in each example shows the motion stream output and the final segmentation result. The other rows are the reset ( $r_t$ ) and the inverse of the update ( $1 - z_t$ ) gate activations for the corresponding  $i$ th dimension. These activations are shown as grayscale heat maps, where white denotes a high activation.

We use the unidirectional model with the DeepLab-v1 appearance stream and LDOF optical flow in the following for better clarity. The reset and update gates of the ConvGRU,  $r_t$  and  $z_t$  respectively, are 3D matrices of  $64 \times w/8 \times h/8$  dimension. The overall behavior of ConvGRU is determined by the interplay of these 128 components. We use a selection of the components of  $r_t$  and  $(1 - z_t)$  to interpret the workings of the gates. Our analysis is shown on two frames which correspond to the middle of the *goat* and *dance-twirl* sequences in (a) and (b), respectively in Figure 11.

The outputs of the motion stream alone (left) and the final segmentation result (right) of the two examples are shown in the top row in the figure. The five rows below correspond to one of the 64 dimensions of  $r_t$  and  $(1 - z_t)$ , with  $i$  denoting the dimension. These activations are shown as grayscale heat maps. High values for either of the two activations increases the influence of the previous state of a ConvGRU unit on the new state matrix computation. If both

values are low, the state in the corresponding locations is rewritten with a new value; see equations (3) and (4).

For  $i = 8$ , we observe the update gate being selective based on the appearance information, i.e., it updates the state for foreground objects and duplicates it for the background. Note that motion does not play a role in this case. This can be seen in the example of stationary people (in the background) on the right, that are treated as foreground by the update gate. In the second row, showing responses for  $i = 18$ , both heatmaps are uniformly close to 0.5, which implies that the new features for this dimension are obtained by combining the previous state and the input at time step  $t$ .

In the third row for  $i = 28$ , the update gate is driven by motion. It keeps the state for regions that are predicted as moving, and rewrites it for other regions in the frame. For the fourth row, where  $i = 41$ ,  $r_t$  is uniformly close to 0, whereas  $(1 - z_t)$  is close to 1. As a result, the input is effectively ignored and the previous state is duplicated. In



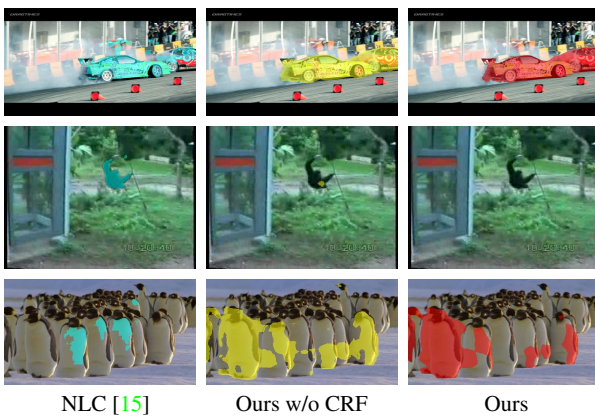


**Fig. 10** Qualitative comparison of two variants of our method with the top-performing approach on SegTrack. Left to right: results of NLC [15], our method without CRF post-processing, and our full method.

the last row showing  $i = 63$ , a more complex behavior can be observed, where the gates rewrite the memory for regions in object boundaries, and use both the previous state and the current input for other regions in the frame.

## 7 Conclusion

This paper introduces a novel approach for video object segmentation. Our method combines two complementary sources of information: appearance and motion, with a visual memory module, realized as a bidirectional convolutional gated recurrent unit. To separate object motion from camera motion we introduce a CNN-based model, which is trained using synthetic data to segment independently moving objects in a flow field. The ConvGRU module encodes spatio-temporal evolution of objects in a video based on a state-of-the-art appearance representation, and uses this encoding to improve motion segmentation. The effectiveness of our approach is validated on three benchmark datasets. We plan to explore instance-level video object segmentation as part of future work.

**Acknowledgements** This work was supported in part by the ERC advanced grant ALLEGRO, a Google research award, a Facebook and an Intel gift. We gratefully acknowledge the support of NVIDIA with the donation of GPUs used for this work. We also thank Yeong Jun Koh for providing segmentation masks produced by their method [34] on the FBMS dataset.

## References

- Adelson, E.H.: On seeing stuff: The perception of materials by humans and machines. *Proc. SPIE* (2001)
- Badrinarayanan, V., Galasso, F., Cipolla, R.: Label propagation in video sequences. In: *CVPR* (2010)
- Ballas, N., Yao, L., Pal, C., Courville, A.: Delving deeper into convolutional networks for learning video representations. In: *ICLR* (2016)
- Bideau, P., Learned-Miller, E.G.: It’s moving! A probabilistic model for causal motion segmentation in moving camera videos. In: *ECCV* (2016)
- Brendel, W., Todorovic, S.: Video object segmentation by tracking regions. In: *ICCV* (2009)
- Brox, T., Malik, J.: Object segmentation by long term analysis of point trajectories. In: *ECCV* (2010)
- Brox, T., Malik, J.: Large displacement optical flow: Descriptor matching in variational motion estimation. *PAMI* **33**(3), 500–513 (2011)
- Caelles, S., and J. Pont-Tuset, K.K.M., Leal-Taixé, L., Cremers, D., Van Gool, L.: One-shot video segmentation. In: *CVPR* (2017)
- Chen, L.C., Papandreou, G., Kokkinos, I., Murphy, K., Yuille, A.L.: Semantic image segmentation with deep convolutional nets and fully connected CRFs. In: *ICLR* (2015)
- Chen, L.C., Papandreou, G., Kokkinos, I., Murphy, K., Yuille, A.L.: Deeplab: Semantic image segmentation with deep convolutional nets, atrous convolution, and fully connected CRFs. *PAMI* (2017)
- Cho, K., van Merriënboer, B., Gülçehre, Ç., Bougares, F., Schwenk, H., Bengio, Y.: Learning phrase representations using RNN encoder-decoder for statistical machine translation. In: *EMNLP* (2014)
- Donahue, J., Hendricks, L.A., Guadarrama, S., Rohrbach, M., Venugopalan, S., Saenko, K., Darrell, T.: Long-term recurrent convolutional networks for visual recognition and description. In: *CVPR* (2015)
- Dosovitskiy, A., Fischer, P., Ilg, E., Häusser, P., Hazırbaş, C., Golkov, V., van der Smagt, P., Cremers, D., Brox, T.: FlowNet: Learning optical flow with convolutional networks. In: *ICCV* (2015)
- Everingham, M., Van Gool, L., Williams, C.K.I., Winn, J., Zisserman, A.: The PASCAL Visual Object Classes Challenge 2012 (VOC2012) Results. <http://www.pascal-network.org/challenges/VOC/voc2012/workshop/index.html>
- Faktor, A., Irani, M.: Video segmentation by non-local consensus voting. In: *BMVC* (2014)
- Finn, C., Goodfellow, I., Levine, S.: Unsupervised learning for physical interaction through video prediction. In: *NIPS* (2016)
- Fragkiadaki, K., Zhang, G., Shi, J.: Video segmentation by tracing discontinuities in a trajectory embedding. In: *CVPR* (2012)
- Glorot, X., Bengio, Y.: Understanding the difficulty of training deep feedforward neural networks. In: *AISTATS* (2010)
- Graves, A.: Generating sequences with recurrent neural networks. arXiv preprint arXiv:1308.0850 (2013)
- Graves, A., Jaitly, N., Mohamed, A.: Hybrid speech recognition with deep bidirectional LSTM. In: *Workshop on Automatic Speech Recognition and Understanding* (2013)
- Graves, A., Mohamed, A., Hinton, G.: Speech recognition with deep recurrent neural networks. In: *ICASSP* (2013)
- Graves, A., Schmidhuber, J.: Framewise phoneme classification with bidirectional LSTM and other neural network architectures. *Neural Networks* **18**(5), 602–610 (2005)
- Grundmann, M., Kwatra, V., Han, M., Essa, I.: Efficient hierarchical graph based video segmentation. In: *CVPR* (2010)
- Hochreiter, S.: The vanishing gradient problem during learning recurrent neural nets and problem solutions. *Int. J. Uncertainty, Fuzziness and Knowledge-Based Systems* **6**(2), 107–116 (1998)
- Hochreiter, S., Schmidhuber, J.: Long short-term memory. *Neural computation* **9**(8), 1735–1780 (1997)
- Hopfield, J.J.: Neural networks and physical systems with emergent collective computational abilities. *Proc. National Academy of Sciences* **79**(8), 2554–2558 (1982)

27. Huguet, F., Devernay, F.: A variational method for scene flow estimation from stereo sequences. In: ICCV (2007)
28. Ilg, E., Mayer, N., Saikia, T., Keuper, M., Dosovitskiy, A., Brox, T.: FlowNet 2.0: Evolution of optical flow estimation with deep networks. In: CVPR (2017)
29. Ioffe, S., Szegedy, C.: Batch normalization: Accelerating deep network training by reducing internal covariate shift. In: ICML (2015)
30. Jain, S.D., Xiong, B., Grauman, K.: Fusionseg: Learning to combine motion and appearance for fully automatic segmentation of generic objects in videos. In: CVPR (2017)
31. Keuper, M., Andres, B., Brox, T.: Motion trajectory segmentation via minimum cost multicut. In: ICCV (2015)
32. Khoreva, A., Galasso, F., Hein, M., Schiele, B.: Classifier based graph construction for video segmentation. In: CVPR (2015)
33. Khoreva, A., Perazzi, F., Benenson, R., Schiele, B., Sorkine-Hornung, A.: Learning video object segmentation from static images. In: CVPR (2017)
34. Koh, Y.J., Kim, C.S.: Primary object segmentation in videos based on region augmentation and reduction. In: CVPR (2017)
35. Krähenbühl, P., Koltun, V.: Efficient inference in fully connected CRFs with Gaussian edge potentials. In: NIPS (2011)
36. Lee, Y.J., Kim, J., Grauman, K.: Key-segments for video object segmentation. In: ICCV (2011)
37. Lezama, J., Alahari, K., Sivic, J., Laptev, I.: Track to the future: Spatio-temporal video segmentation with long-range motion cues. In: CVPR (2011)
38. Li, F., Kim, T., Humayun, A., Tsai, D., Rehg, J.M.: Video segmentation by tracking many figure-ground segments. In: ICCV (2013)
39. Lin, T.Y., Maire, M., Belongie, S., Hays, J., Perona, P., Ramanan, D., Dollár, P., Zitnick, C.L.: Microsoft COCO: Common objects in context. In: ECCV (2014)
40. Long, J., Shelhamer, E., Darrell, T.: Fully convolutional networks for semantic segmentation. In: CVPR (2015)
41. Mayer, N., Ilg, E., Häusser, P., Fischer, P., Cremers, D., Dosovitskiy, A., Brox, T.: A large dataset to train convolutional networks for disparity, optical flow, and scene flow estimation. In: CVPR (2016)
42. Mikolov, T., Karafiát, M., Burget, L., Cernocký, J., Khudanpur, S.: Recurrent neural network based language model. In: Interspeech (2010)
43. Narayana, M., Hanson, A.R., Learned-Miller, E.G.: Coherent motion segmentation in moving camera videos using optical flow orientations. In: ICCV (2013)
44. Ng, J.Y., Hausknecht, M.J., Vijayanarasimhan, S., Vinyals, O., Monga, R., Toderici, G.: Beyond short snippets: Deep networks for video classification. In: CVPR (2015)
45. Ochs, P., Brox, T.: Higher order motion models and spectral clustering. In: CVPR (2012)
46. Ochs, P., Malik, J., Brox, T.: Segmentation of moving objects by long term video analysis. PAMI **36**(6), 1187–1200 (2014)
47. Papazoglou, A., Ferrari, V.: Fast object segmentation in unconstrained video. In: ICCV (2013)
48. Pascanu, R., Mikolov, T., Bengio, Y.: On the difficulty of training recurrent neural networks. In: ICML (2013)
49. Patraucean, V., Handa, A., Cipolla, R.: Spatio-temporal video autoencoder with differentiable memory. In: ICLR Workshop track (2016)
50. Perazzi, F., Pont-Tuset, J., McWilliams, B., van Gool, L., Gross, M., Sorkine-Hornung, A.: A benchmark dataset and evaluation methodology for video object segmentation. In: CVPR (2016)
51. Pinheiro, P.O., Lin, T.Y., Collobert, R., Dollár, P.: Learning to refine object segments. In: ECCV (2016)
52. Ren, S., He, K., Girshick, R., Sun, J.: Faster R-CNN: Towards real-time object detection with region proposal networks. In: NIPS (2015)
53. Revaud, J., Weinzaepfel, P., Harchaoui, Z., Schmid, C.: EpicFlow: Edge-preserving interpolation of correspondences for optical flow. In: CVPR (2015)
54. Ronneberger, O., Fischer, P., Brox, T.: U-Net: Convolutional networks for biomedical image segmentation. In: MICCAI (2015)
55. Rumelhart, D.E., Hinton, G.E., Williams, R.J.: Learning representations by back-propagating errors. Nature **323**, 533–536 (1986)
56. Russakovsky, O., Deng, J., Su, H., Krause, J., Satheesh, S., Ma, S., Huang, Z., Karpathy, A., Khosla, A., Bernstein, M., Berg, A.C., Fei-Fei, L.: Imagenet large scale visual recognition challenge. IJCV **115**(3), 211–252 (2015)
57. Shi, X., Chen, Z., Wang, H., Yeung, D.Y., Wong, W., Woo, W.: Convolutional LSTM network: A machine learning approach for precipitation nowcasting. In: NIPS (2015)
58. Simonyan, K., Zisserman, A.: Two-stream convolutional networks for action recognition in videos. In: NIPS (2014)
59. Srivastava, N., Mansimov, E., Salakhutdinov, R.: Unsupervised learning of video representations using LSTMs. In: ICML (2015)
60. Sundaram, N., Brox, T., Keutzer, K.: Dense point trajectories by GPU-accelerated large displacement optical flow. In: ECCV (2010)
61. Taylor, B., Karasev, V., Soatto, S.: Causal video object segmentation from persistence of occlusions. In: CVPR (2015)
62. Tieleman, T., Hinton, G.: RMSProp. COURSERA: Lecture 6.5 - Neural Networks for Machine Learning (2012)
63. Tokmakov, P., Alahari, K., Schmid, C.: Learning motion patterns in videos. In: CVPR (2017)
64. Tokmakov, P., Alahari, K., Schmid, C.: Learning video object segmentation with visual memory. In: ICCV (2017)
65. Torr, P.H.S.: Geometric motion segmentation and model selection. Phil. Trans. Royal Society of London A: Mathematical, Physical and Engineering Sciences **356**(1740), 1321–1340 (1998)
66. Vedula, S., Baker, S., Rander, P., Collins, R., Kanade, T.: Three-dimensional scene flow. PAMI **27**(3), 475–480 (2005)
67. Vogel, C., Schindler, K., Roth, S.: 3D scene flow estimation with a piecewise rigid scene model. IJCV **115**(1), 1–28 (2015)
68. Wang, W., Shen, J., Porikli, F.: Saliency-aware geodesic video object segmentation. In: CVPR (2015)
69. Wedel, A., Brox, T., Vaudrey, T., Rabe, C., Franke, U., Cremers, D.: Stereoscopic scene flow computation for 3D motion understanding. IJCV **95**(1), 29–51 (2011)
70. Werbos, P.J.: Backpropagation through time: What it does and how to do it. Proc. IEEE **78**(10), 1550–1560 (1990)
71. Xu, C., Corso, J.J.: Libsvx: A supervoxel library and benchmark for early video processing. International Journal of Computer Vision **119**(3), 272–290 (2016)
72. Zhang, D., Javed, O., Shah, M.: Video object segmentation through spatially accurate and temporally dense extraction of primary object regions. In: CVPR (2013)